Near-wall dynamics of compressible boundary layers

Maher Lagha, John Kim, Jeff D. Eldredge, and Xiaolin Zhong
Mechanical and Aerospace Engineering Department, UCLA, 420 Westwood Plaza, Los Angeles, California 90095-1597, USA

(Received 11 February 2011; accepted 26 May 2011; published online 20 June 2011)

The coherent structures populating the inner-region of a compressible boundary layer with free-stream Mach number equal to 2.5 are analyzed by means of direct numerical simulations of the Navier–Stokes equations. This study shows similarity with the incompressible case in the sense that turbulence in the near-wall region can be sustained without fluctuations in the outer region, proving the existence of a local cycle within the near-wall region. The dynamics are further simplified by making use of the coherence of the inner region. The wall-normal velocity component in this region is split into two: one coherent part representing vortices spanning all the inner-region, and one incoherent part representing the background turbulence. By damping the latter part, the statistical features of the flow are only slightly influenced, showing that the coherent part is essential in determining the flow characteristics. Flow dynamics and turbulence structures within this coherent part are examined. It is shown that the near-wall region is populated by crescent-shaped vortical structures, which are associated with regions with strong positive Reynolds shear stress production. The structure of the flow associated with these regions shares several features with the so-called internal shear layers. © *2011 American Institute of Physics*. [doi:10.1063/1.3600659]

I. INTRODUCTION

Turbulent boundary-layer flow displays a symbiosis of organized motions known as coherent structures. The knowledge of their kinematic properties, such as sizes and shapes, as well as their dynamical properties, such as origin and stability, is the key point to understanding the self-sustainment of the near-wall turbulence. Due to a great deal of experimental and numerical work conducted over the past few decades, it is now well known that the near-wall region is populated by streaks and streamwise vortices, which are the coherent structures responsible for turbulence production near the wall (Refs. 1, 2 and references therein).

However, our knowledge of these structures is still limited.

From a dynamical point of view, the generation mechanism of these streamwise vortices is still an open question. For a complete collection of the proposed mechanisms, the interested reader is referred to the review by Panton.[1] On the other hand, some of the kinematic properties of these structures are still a source of debate. In particular, there is still no consensus on whether they occur in counter-rotating pairs, as they are imagined by extending the hairpin vortex paradigm of Theodorsen down to the near-wall region (e.g., Ref. 2), or staggered in the streamwise direction (e.g., Ref. 3). The origin of the difference between these conceptual models is an interesting study in itself. However, once educed, the significance of these vortices has to be measured based on their contribution to the production of turbulent kinetic energy.

In this paper, we address the two-fold question concerning the shape and the dynamical significance of the vortices in the near-wall region. This question is tackled by first educing the vortices and then by evaluating their importance in terms of their contribution to the Reynolds shear stress and energy production. The second point is achieved by isolating the contribution of the coherent turbulent part from that of the incoherent part. A similar approach was used in the study of incompressible turbulent channel flow by Jimenez and Pinelli[4,5] In that study, the coherent part, i.e., the streaks was damped to show that turbulence cannot sustain without streaks. In contrast, this study actively damps the incoherent part of the velocity. The turbulence is sustained and the statistical features of the flow are left essentially intact and allow us to easily study the coherent part and evaluate its contribution.

We study the near-wall region of compressible turbulent boundary layers, defined from $y^+=0$ up to $y^+=60$. Here $y^+=yu_\tau/\nu_w$ and the superscript "+" denotes normalization by viscous units. The kinematic viscosity is ν_w, $u_\tau=\sqrt{\tau_w/\rho_w}$ is the friction velocity, τ_w is the wall shear stress, and ρ_w is the density at the wall. Note that based on our previous result (Ref. 6, referred to as Part I hereinafter), there is likely no difference in the structure of compressible and incompressible turbulent flow. In fact, for a free-stream Mach number ranging from 2.5 to 20 and using perfect gas assumption, we have shown that scaled statistics of the compressible flow collapsed with the statistics of the incompressible flow. In addition, near-wall streaks and streamwise vortices have been commonly observed in other direct numerical simulations (DNS) of compressible turbulent boundary layer for different freestream Mach numbers ($M_\infty=3$, in Ref. 7 and $M_\infty=2.25$ in Ref. 8). Both studies revealed similar coherent structures as observed in subsonic and supersonic experiments, i.e., elongated streaky structures of alternating high- and low-speed fluid in the near-wall region, and hairpin vortex packets frequently located above low-speed streaks. Furthermore, Pirozzoli *et al.*[8] showed that the viscous sublayer and the buffer layer are mostly

populated by quasi-streamwise vortices and that the population of clockwise and counterclockwise cores is nearly the same.

A. Goal and organization of the paper

Our main goal is to draw a simplified picture of the dynamics of the coherent structures populating the near-wall region of compressible boundary layers. The direct numerical simulations of these boundary layers were carried out in Part I. Therefore, all the notations are identical to those defined there. The adiabatic boundary condition is used at the wall.

The paper is organized as follows. In Sec. II, we demonstrate, by filtering out the turbulence above $y^+ \approx 60$, the existence of a self-sustained cycle within the near-wall region. This filtered flow field will be referred to as the flow field of step 2, in contrast with the unfiltered flow field of Part I referred to as the flow field of step 1. The different nomenclatures are given in Table I. We then show that the dynamics of the turbulent flow field in the near-wall region can be approximated by the coherent part of the wall-normal velocity, while the incoherent part is damped out. The obtained flow field is referred to as the flow field of step 3. We demonstrate that this approach can successfully capture the complex flow features (e.g., rms values) with much simpler dynamics, since the coherent structures are much easier to identify and track without the need of a complex post-processing method. Our approach clarifies the turbulence structure and gives valuable insight into the mechanisms.

The discussion of the results and their comparisons with previous studies are presented in Sec. IV. The conclusion is given in Sec. V. In this paper, we use x, y, z to denote the streamwise, wall-normal, and spanwise directions, respectively, and u, v, w to denote the velocity components in x, y, and z directions.

II. STUDY OF THE NEAR-WALL REGION

We will first demonstrate the existence of a self-sustained cycle for turbulence in the near-wall region of the supersonic boundary layer ($M_\infty = 2.5$). Then we will isolate the vortices populating this region.

A. Existence of a cycle in the near-wall region ($y^+ \leq 60$)

Jimenez and Pinelli[4] have shown the existence of an autonomous cycle in the near-wall region by damping all the perturbations above the inner-region ($y^+ \geq 60$). A similar approach is used here for the compressible flow. However, we have found that damping the wall-normal velocity v is sufficient to damp all the perturbations above the near-wall region. The quantity $-F(y)(v - \bar{v})$ is added to the right-hand side of the v-equation, where $\bar{v}$ is the spanwise mean profile of v. The function F that we use, shown in Fig. 1, is

$$F(y) = \begin{cases} 0, & y \leq y_{y^+=60} \\ \sigma \dfrac{(y - y_{y^+=60})^n (L_y - y)}{(L_y - y_{y^+=60})^{n+2}}, & y \geq y_{y^+=60} \end{cases}$$

where σ and n are two adjustable parameters,[9,10] and $y_{y^+=60}$ denotes the physical location which corresponds to $y^+ = 60$. A generic time step for v

$$v(x, y, z, t + \Delta_t) = v(x, y, z, t) + \Delta_t \, \mathrm{rhs_v}$$

becomes

$$v(x, y, z, t + \Delta_t) = v(x, y, z, t) + \Delta_t \, \mathrm{rhs_v} - F(y)(v(x, y, z, t) - \bar{v}),$$

where Δt is the integration time step and $\mathrm{rhs_v}$ is the right-hand side in the v-equation.

Note that the governing equations are integrated in a conservative form, ρv, but the filter is applied to v only. Different values of the filter parameter n (and therefore different forms of the filter F) give similar results, therefore only the results for one filter ($n = 3$, $\sigma = 25$) are presented in this paper.

After a short transient during which all the fluctuations above $y^+ = 60$ are mostly damped, the turbulent flow in the inner region survives and settles to $R_\tau \approx 324$, close to the unfiltered $R_\tau \approx 350$. The domain extent in wall units remain similar to that of the unfiltered simulation: $L_x^+ \times L_y^+ \times L_z^+ \approx 4100 \times 500 \times 760$ (Part I). It is worth mentioning that Jimenez and Pinelli have seen a similar but more important drop in the wall shear, and the Reynolds number dropped from $R_\tau \approx 200$ to 100.

Note that $y^+ = 60$ corresponds in the physical domain to $y/\delta_{99} \approx 0.16$. Due to a small drop in the friction at the wall,

TABLE I. Nomenclatures used in the text.

Case	Definition
Step 1	Reference (unfiltered) flow field from Part I
Step 2	Damping all perturbations for $y^+ \geq 60$ of the flow field in step 1
Step 3	Galerkin projection of the v' velocity of the flow field in step 2

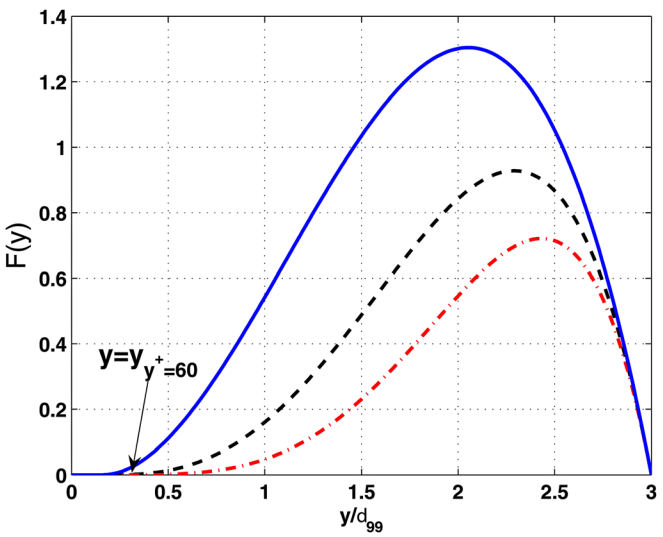

FIG. 1. (Color online) Examples of the filter $F(y)$, with $n = 2$ (solid line), $n = 3$ (dashed line), and $n = 4$ (dash-dotted line).

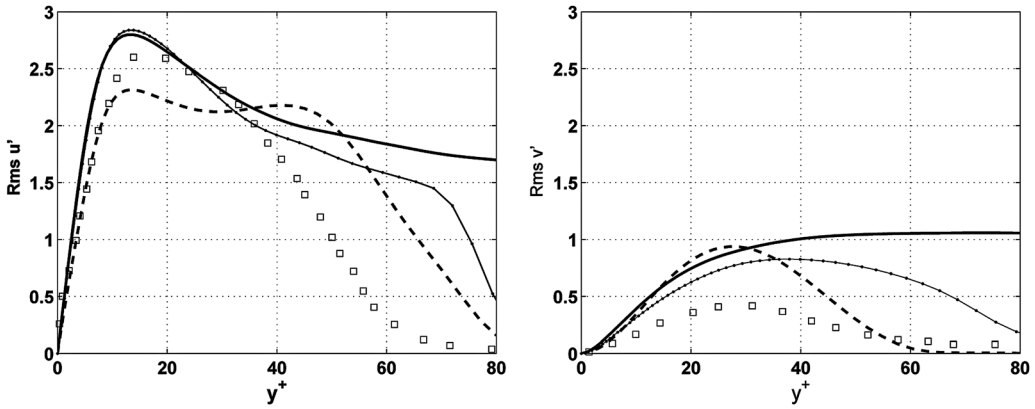

FIG. 2. Reynolds normal stress components for steps 1, 2, and 3. Lines correspond to the current simulations and squares to Jimenez and Pinelli filtered results (Ref. 4). Thick solid line: step 1. Thin solid line: step 2. Dashed line: step 3.

the physical location corresponding to $y^+ = 60$ will change slightly. In fact, the non-dimensional friction velocity drops from $u_\tau/U_\infty \approx 0.053$ to 0.045, and therefore the viscous unit increases (at roughly constant $\nu_w/\nu_\infty \approx 3.86$) and the physical location becomes $y/\delta_{99} \approx 0.19$. Fixing the location of the filter in terms of wall unit ($y^+ \approx 60$) or physical unit ($y \in [0.16, 0.19]$) gives similar root-mean-square (rms) distributions. Most importantly, the following results about the coherent structures are not affected.

The rms fluctuations of the velocity components are given in Figs. 2 and 3. The near-wall profiles are similar to those of step 1.

The rms fluctuations of the vorticity components are given in Figs. 4 and 5, together with the turbulent Mach number (see Part I for the definition). While the rms fluctuations in Jimenez and Pinelli are strongly affected (except for u' and ω_y'), here most of them are not affected by the filtering process. Jimenez and Pinelli attribute this sensitivity to the fact that the streamwise vortices, due to their less energetic velocities, are more sensitive to filtering.

Note that even if the rms of v' is reduced, the production term in the turbulent-kinetic-energy budget is almost the same, as shown in Fig. 6. Hence, the velocity fluctuations of the filtered flow as well as the kinetic energy budget are very close to the unfiltered results of Part 1, thus demonstrating that an outer flow is not needed for the maintenance of near-wall turbulence, or even for defining its quantitative properties. This illustrates the existence of a local self-sustaining process for the turbulence in the inner region in compressible turbulent boundary layers.

B. A Galerkin projection of near-wall structures

Our aim is to shed some light on the coherent structures populating the inner-region and examine their dynamics in a simplified situation in which their interactions with the outer flow are damped. In this section, we show that this can be achieved by using the coherence of the inner region, which constitutes, once isolated from the outer region, a confined system in the y-direction.

By considering short domains with respect to the typical longitudinal extent of the streaks and therefore systems confined in the x-direction, Jimenez and Pinelli gave an approximate representation of the streaks by that part of the streamwise velocity perturbation u', which depends on the transverse coordinates, y and z, but independent of x. They defined the streak component as the streamwise average of u' and decomposed u' into a streak component (coherent part) and background turbulence (incoherent part). Considering the streaks as the average of the velocity is a first order approximation (first harmonic), the higher harmonics are included in the incoherent part. A similar approach is applied

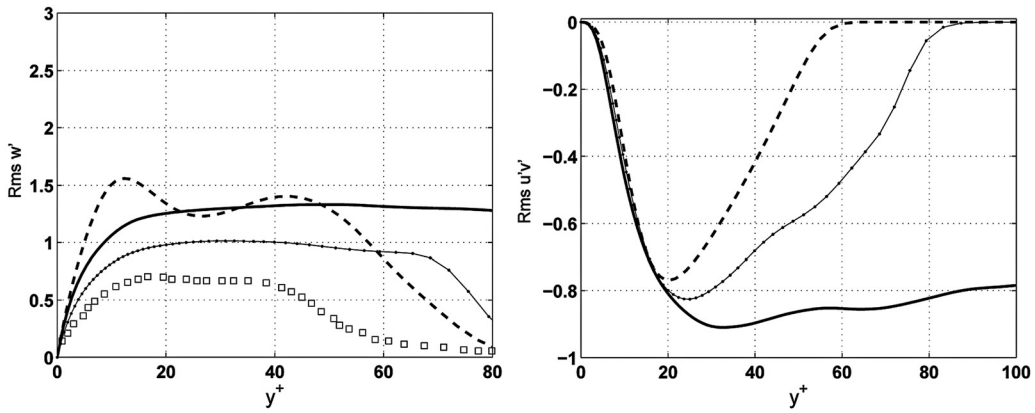

FIG. 3. Reynolds shear stress components for steps 1, 2, and 3. Legend similar to Fig. 2.

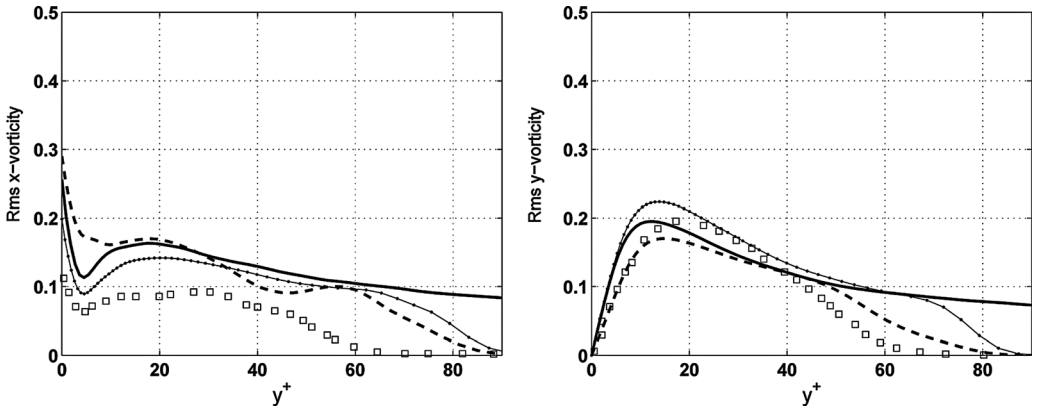

FIG. 4. rms vorticity components for steps 1, 2, and 3. Lines correspond to the current simulations and symbols to Jimenez and Pinelli filtered results (Ref. 4). Legend similar to Fig. 2.

here but to the streamwise vortices. The main idea is based on the fact that these structures are coherent and span the entire inner region $y^+ \in [0, 60]$ with the core's location around $y^+ \approx 20$. We decompose the wall-normal velocity perturbation into a coherent "vortical" component and an "incoherent" component

$$v'(x, y, z, t) = v'_{\text{vor}}(x, y, z, t) + v'_{\text{inc}}(x, y, z, t).$$

The velocity component associated with these vortices is defined as

$$v'_{\text{vor}}(x, y, z, t) = P_1(y) v'_1(x, z, t),$$
$$v'_1(x, z, t) = \int_0^{y_y^+=60} P_1(y) v'(x, y, z, t)\, dy,$$

where P_1 is a polynomial function vanishing at $y = 0$ and $y = y_{y^+=60}$ and with a maximum around $y^+ \approx 20$. At $y^+ = 60$, we have chosen $\frac{d^2 P_1}{dy^2} = 0$ to guarantee a smooth transition to the outer region where v' is zero. Therefore the considered function is $P_1(y) = y^2 \left(y - y_{y^+=60}\right)^3$. Once v'_{vor} is computed, the incoherent part is obtained as $v'_{\text{inc}} = v' - v'_{\text{vor}}$.

It is worth noting that the amount of energy contained in this mode, defined as

$$E_1 = \int_{y=0}^{y=y_{y^+=60}} v'^2_{\text{vor}}(x, y, z, t) dy,$$

is about 60% of the wall-normal turbulent kinetic energy $E_0 = \int_{y=0}^{y=y_{y^+=60}} v'^2 dy$, showing that this first mode captures more than half of the energy. Even if this single mode captures only 60% of the energy, we will show that when isolated from the incoherent part v'_{inc} (i.e., other small-scale structures) it is sufficient to capture most of the turbulence production. Using different forms of functions or including additional modes may increase this percentage, but the goal of this paper is not to reproduce the statistics but rather to understand the dynamics.

In the spirit of the remark made about the harmonics in the definition of the streaks by Jimenez and Pinelli, the approximation made above for the wall-normal velocity associated with the vortices spanning the near-wall region can be seen as a first-order approximation in a Galerkin projection. This method is usually applied to structures in confined systems, where a few (wall-normal) modes are sufficient to capture them. Therefore P_1 constitutes the first mode of such an expansion. This restriction can be overcome by adding more harmonics, but we are mostly looking for qualitative clues about the dynamics rather than quantitative agreement.

C. Explicit projection

To show that the presence of the streaks is essential to the production of turbulence, Jimenez and Pinelli decomposed u' into one coherent part (streaks) and one incoherent

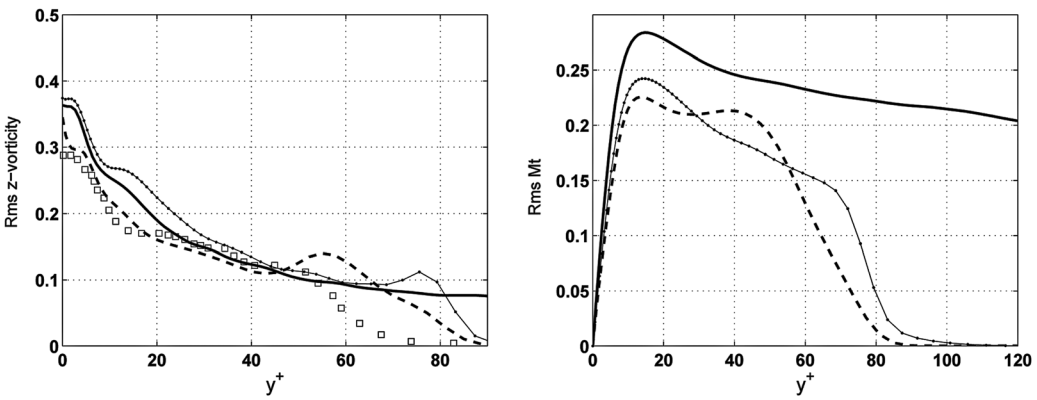

FIG. 5. Left: rms of the spanwise vorticity component for steps 1, 2, and 3. Right: turbulent Mach number. Legend similar to Fig. 4.

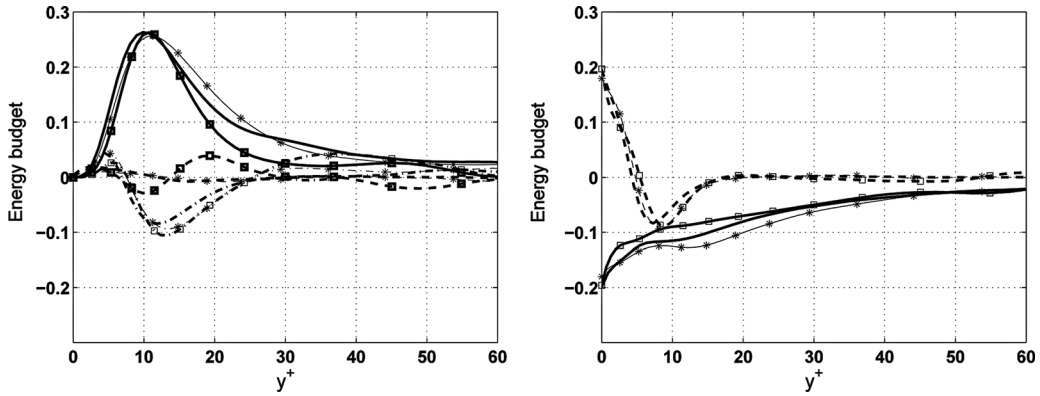

FIG. 6. Kinetic energy budget. Left: production P (—), transport T (-.-.), pressure term Π (- - -). Right: viscous diffusion D (- - -) and viscous dissipation $-\Phi$ (—). Line with no symbols: step 1. Line with stars: step 2. Line with squares: step 3.

part and damped the streaks component by multiplying it by a filter function at every time step of the numerical integration. As expected, without the streaks, the turbulence decayed. We use a similar approach here but applied to the wall-normal perturbation v'. Rather than merely showing that the turbulence decays by damping the coherent part and hence that vortices are essential to the turbulence cycle, we isolate the vortices from the incoherent part by explicitly damping the latter. This is expected to give a simple picture of the vortices dynamics.

The equations of motion are integrated as usual, but at each time step v' is separated into the two parts, $v' = v'_{\text{vor}} + v'_{\text{inc}}$, and v'_{inc} is removed. The turbulent flow obtained through this projection is referred to as the flow of step 3 and is analyzed below.

First and foremost, the turbulence remains self-sustained when this procedure is carried out. This illustrates that only vortices spanning the entire gap are essential to turbulence production. The features of the obtained turbulent flow field are in reasonable agreement with those of step 1 and step 2, as shown in Figs. 2–6. The Reynolds number R_τ and the friction velocity are roughly the same as in step 2. Therefore, the spatial extent of the domain in wall units is almost unchanged.

It is interesting to note that the obtained profiles of velocity fluctuations have similar shape to those of Jimenez and Pinelli. The streamwise velocity has two bumps; the one closer to the wall is higher than the other. The wall-normal velocity has a similar shape, a direct signature of a vortex, but with amplitude closer to the real flow than in Jimenez and Pinelli. The rms of the spanwise velocity w' is slightly higher but also shows the same two-bump pattern. This pattern can be easily explained by the presence of the streamwise vortices. The maximum near the wall is higher for w', since w' increases near the wall before going to zero. Also, the amplitude of this maximum is slightly larger than the rms of the non-projected flow, since in this highly constrained flow the location of the core of the vortex stays at a constant distance from the wall, while in a real turbulent flow the wandering of this vortex gives lower rms values. The rms of the vorticity component fluctuations show the same robustness and are very close to the real flow. The same observation holds for the kinetic energy budget, as shown in Fig. 6.

Finally, the distributions of the van Driest-transformed mean streamwise velocity for steps 1, 2, and 3 are shown in a semi-logarithmic plot in Fig. 7. The linear scaling in the viscous sublayer $\left(u^+_{vd} = y^+\right)$ and the logarithmic scaling in the overlap region $\left(y^+_{\text{vd}} = (1/k)\log y^+ + 5.1,\ k \approx 0.4\right)$ are also plotted as references.

D. Instantaneous structures

Having shown that the flow field of step 3 is statistically similar to step 1 and step 2, instantaneous flow fields of step 3 are analyzed in this section. Figure 8 shows a typical velocity field plot of the instantaneous velocity fluctuation v' at $y^+ = 15$. In this figure the flow is from left to right. The most recognizable pattern has a crescent shape. Each one corresponds to two counter-rotating vortices, as revealed by the cross-stream section (y-z) of the flow field (v', w') in Fig. 9. Positive patches of v' corresponds to negative patches of u' and vice versa. This $u'v'$-anticorrelation, which gives positive Reynolds shear stress $-u'v'$, is associated with the so-called lift-up mechanism.[11]

The induced positive and negative u' fluctuations via this mechanism correspond, respectively, to high and low

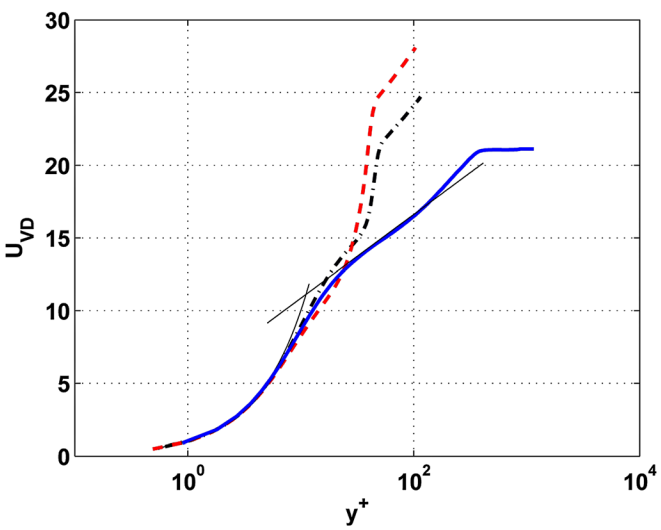

FIG. 7. (Color online) Plots of the van Driest transformed mean velocity profiles for step 1 (solid line), step 2 (dash dotted line), step 3 (dashed line).

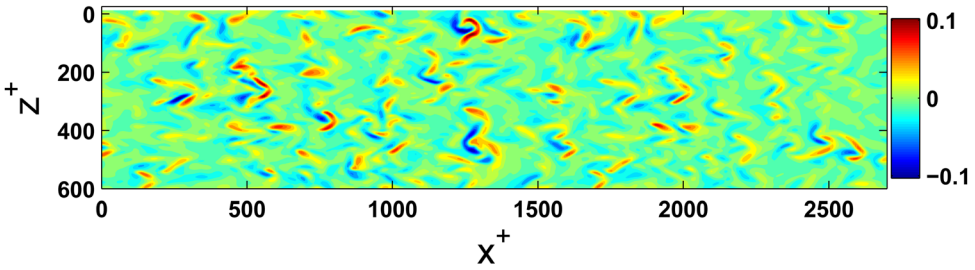

FIG. 8. (Color online) Spatial distribution of the wall-normal velocity at $y^+ \approx 15$ in a (x^+, z^+)-plane (enhanced online). [URL: http://dx.doi.org/10.1063/1.3600659.1]

speed streaks. These streaks span the entire near-wall region up to $y^+ \approx 60$ (Fig. 9).

The density and temperature fluctuations, ρ' and T', corresponding to this typical crescent vortex are given in Fig. 10. Away from the wall, around $y^+ \approx 15$–25, a region where v' is positive corresponds to a region where T' is positive and vice versa, as one would expect from a "lift-up mechanism" applied to the mean temperature profile. The same observation holds for the density fluctuation (but with an opposite sign). Note that very near the wall, an interesting feature takes place. On a given wall-normal line, say at $z^+ = 230$ in Fig. 10, the temperature fluctuations at $y^+ \approx 3$ have the opposite sign of T' at $y^+ \approx 25$, as also shown in Fig. 11. It is not clear what causes this somewhat unexpected near-wall behavior of the temperature fluctuations. It should be pointed out that this peculiar behavior is not due to the filtering process as it is also observed in the flow of step 1.

The sign of the velocity perturbation v' between the legs of the crescent vortex can be used to classify two kinds of crescent vortices. The first kind is depicted in Fig. 9, where the velocity v' is negative between the legs of the crescent vortex and is positive outside (light-gray crescent contour–red online). The flow structure in the (x, z)-plane, corresponding to the second kind of vortex, and supplemented with a cross-stream section in (y, z)-plane, is shown in Fig. 12. For this vortex, the velocity v' is positive between its legs and is negative outside (dark crescent contour–blue online). This vortex shares several features with the vortex of the first kind. First, it produces positive Reynolds shear stress $-u'v' \geq 0$, since positive (negative) wall normal velocity v' induces negative (positive) streamwise fluctuation u' via the lift-up mechanism. Second, fluid flowing away from the wall ($v' \geq 0$) carries high temperature from the wall towards a cooler region, producing a positive temperature fluctuation $T' \geq 0$, as one would expect from the pure convection of the temperature by the wall-normal velocity, as shown in Fig. 13. The same reasoning can be applied to fluid flowing towards the wall.

The crescent vortices and velocity fields in both the (x, z)- and (z, y)-planes shown in Figs. 9 and 12 come from an individual snapshot, but the patterns are representative of

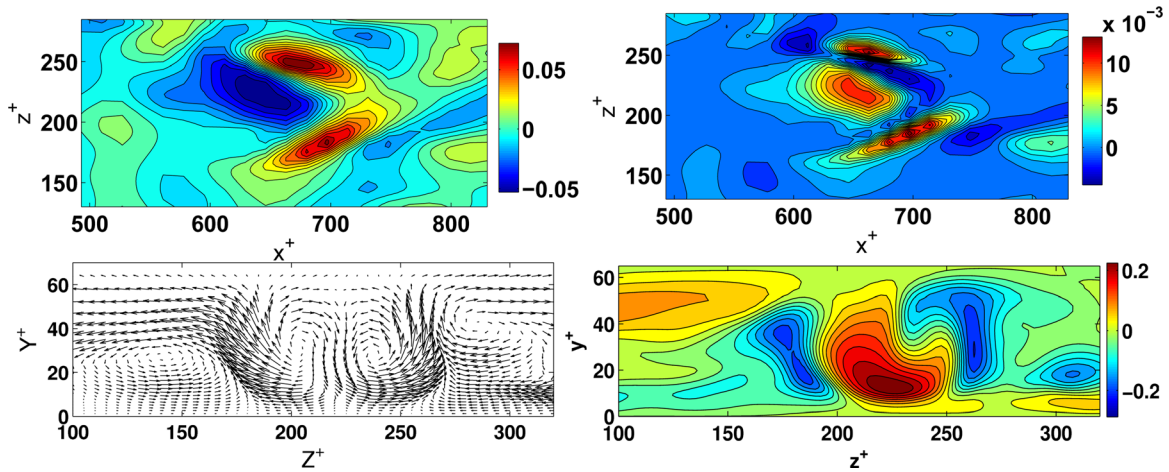

FIG. 9. (Color online) Features of a typical crescent vortex of the first kind. Left to right and top to bottom: (1) spatial distribution of v' at $y^+ \approx 15$; (2) spatial distribution of $-u'v'$ at $y^+ \approx 15$; (3) cross-stream distribution of (v', w') at $x^+ \approx 680$; (4) cross-stream distribution of u'.

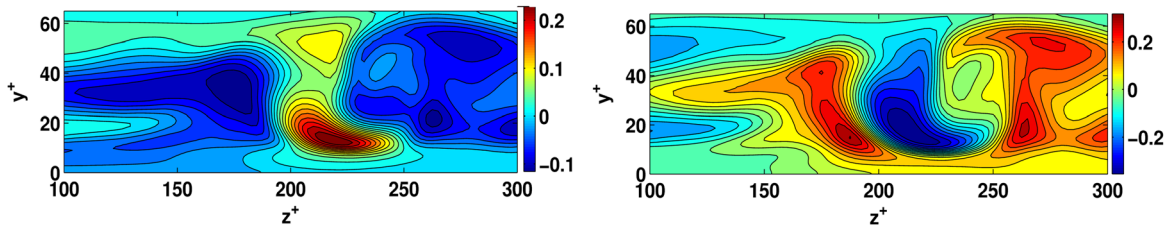

FIG. 10. (Color online) Cross-stream distributions of ρ' (left) and T' (right), corresponding to the crescent vortex shown in Fig. 9.

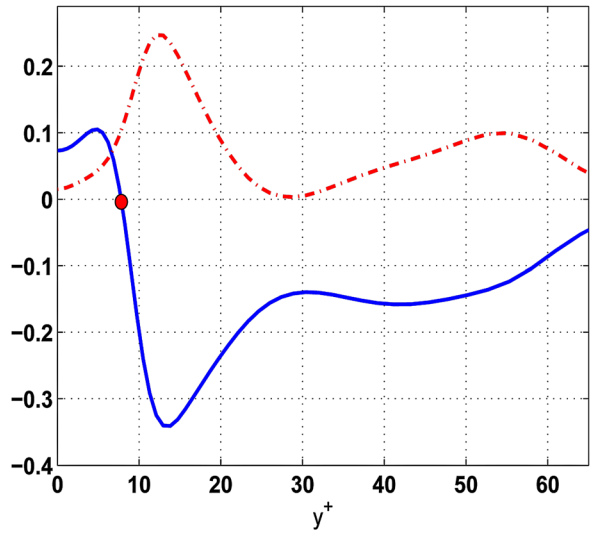

FIG. 11. (Color online) Profiles of the temperature (solid) and density (dash-dotted) fluctuations, along the wall-normal line passing through $z^+ = 230$ in Fig. 10.

those found across the whole field at different times. These flow structures are significant to the turbulent flow dynamics in the near-wall region, since they occur frequently in the flow and are associated with most positive Reynolds shear stress events. Both kinds of crescent vortices and their relation to one another are further considered below.

E. Statistical analysis

Statistical analyses of velocity and vorticity fluctuations were conducted to confirm the validity of the qualitative observations made based on instantaneous fields. Analyses were carried out by locating the regions associated with positive Reynolds shear stress $-u'v'$ and averaging in space across these regions for different times. The statistics for each kind of crescent vortex are first collected separately. This yielded a space-time average of the flow structure corresponding to each kind. Both statistics, depicted in Figs. 14 and 15, show similar features. The (u',w') velocity field fluctuations in the (x, z)-plane reveals a dipolar distribution (a dipole with y-axis) and shows the existence of positive and negative u' fluctuations, corresponding to high and low speed streaks, respectively. These streaks exhibit a characteristic width of approximately 80–100 wall units, they extend a larger distance in the streamwise direction, and they span the entire near-wall region from the wall up to $y^+ \approx 50$–60.

The two counter-rotating streamwise vortices for each crescent vortex are represented by two adjacent patches of positive and negative ω'_x. These patches of ω'_x are connected by a region of positive ω'_z, as shown in Figs. 14 and 15. When rescaling both streamwise and spanwise vorticity using the wall quantities ν_w and u_τ, their amplitudes are similar to the scaled rms values, given in Figs. 4 and 5. The 3D structure of the crescent vortices is now clear: its "legs" represent two counter-rotating streamwise vortices $(\pm\omega'_x)$ while its "head" represents a spanwise vortex with $\omega'_z \geq 0$.

Furthermore, by adding together the statistics of the two kinds of crescent vortices, we obtain a complete space-time average of the fluid structure corresponding to these crescent vortices. As shown in Fig. 16, it consists of a spanwise vortex with positive ω'_z surrounded by a quadrupolar flow field (u', w'). Around this vortex's center, a high-speed streak $u' \geq 0$ impacts a low-speed streak $u' \leq 0$ and results in a stagnation point $u' \approx 0$ with a negative gradient $\partial u'/\partial x \leq 0$ and a positive gradient $\partial_z w' \geq 0$. On each side of this stagnation point $(x^+ \approx 0, z^+ \approx 0)$, there are two patches of $\pm\omega'_x$ but with opposite distributions in the spanwise direction. The distributions of v' and u' around this stagnation point are anti-correlated and provide the positive Reynolds shear stress $-u'\,v' \geq 0$. The structure of the flow around these regions of turbulent kinetic energy production is very similar to that obtained by Johansson *et al.*[12] in channel flow. For example, the structure of the velocity component u' is very similar to the one given in Fig. 5 and 6 in Ref. 12, highlighting a negative $\partial_x u'$ with a stagnation point $u' \approx 0$. Around this point, the v' observed in Figs. 16 has similar topology as in Fig. 5 and 6 in Ref. 12, with $\partial_x v' \geq 0$. This positive gradient of v' is the signature of a spanwise vortex with positive

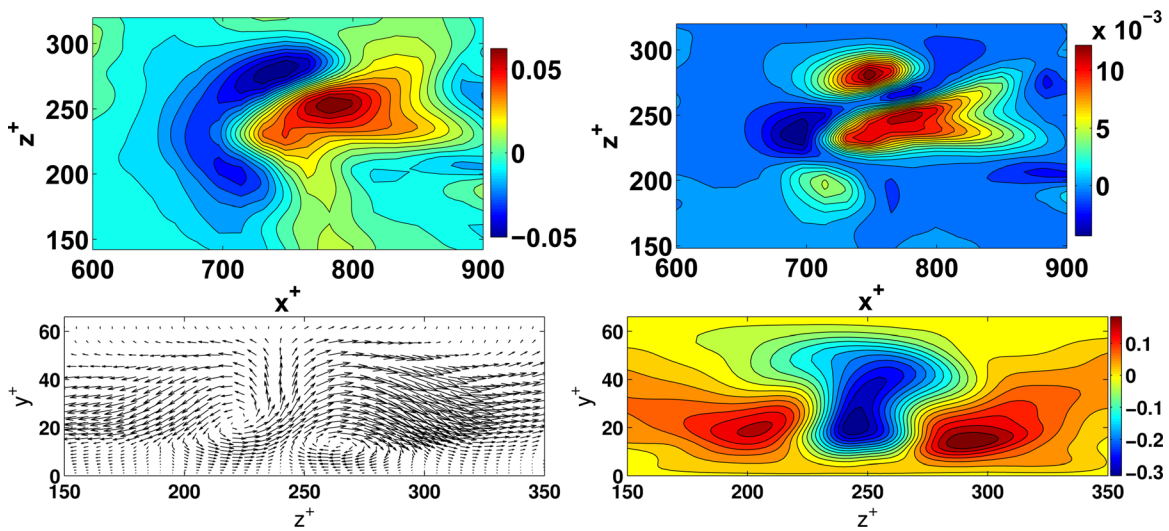

FIG. 12. (Color online) Features of a typical crescent vortex of the second kind. Left to right and top to bottom: (1) spatial distribution of v' at $y^+ \approx 15$; (2) spatial distribution of $-u'v'$ at $y^+ \approx 15$; (3) cross-stream distribution of (v', w'); (4) cross-stream distribution of u'.

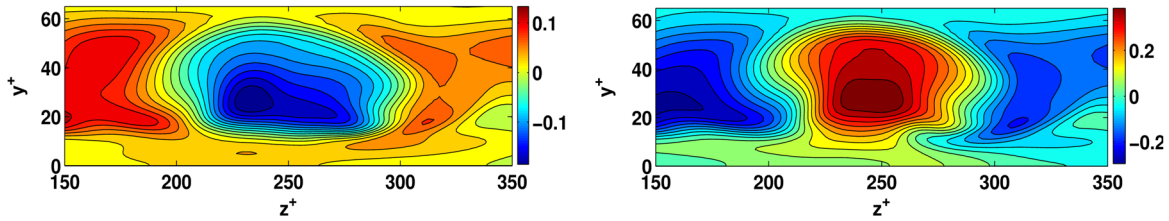

FIG. 13. (Color online) Cross-stream distribution of ρ' (left) and T' (right), corresponding to the crescent vortex shown in Fig. 12.

ω_z', which constitutes the head of crescent vortices. Note that the quadrupolar flow (u', w') is not symmetrical around the stagnation point, as is the case in Ref. 12. This is due to the fact that the symmetry with respect to x in the channel flow simulation in Ref. 12 is absent in the boundary layer flow.

III. A CONCEPTUAL MODEL FOR STREAMWISE VORTICES GENERATION

Streamwise vortices play the essential role in all self-sustaining mechanisms of near-wall turbulence (e.g., Refs. 13, 14). There have been different explanations as to how these vortices are generated and maintained. For example, Hamilton *et al.*[13] reported that the nonlinear advective term, $v'\partial_y\omega_x'$, is primarily responsible for generating streamwise vortices from streamwise-dependent perturbations, while Schoppa and Hussain,[14] asserted that the vortex stretching term, $\omega_x'\partial_x u'$, is primarily responsible for the generation. In this section, we present a comprehensive conceptual model for the generation of streamwise vortices based on the present simulations.

In this model, illustrated in Fig. 17, a spanwise vortex with positive ω_z' is stretched in the spanwise direction due to a positive $\partial_z w'$. This spanwise vortex is then tilted in the streamwise direction by the spanwise shear of the streaks, i.e., $\partial_z u'$, and stretched in the x-direction by the streaks, i.e., $\partial_x u'$, and two streamwise vortices are generated.

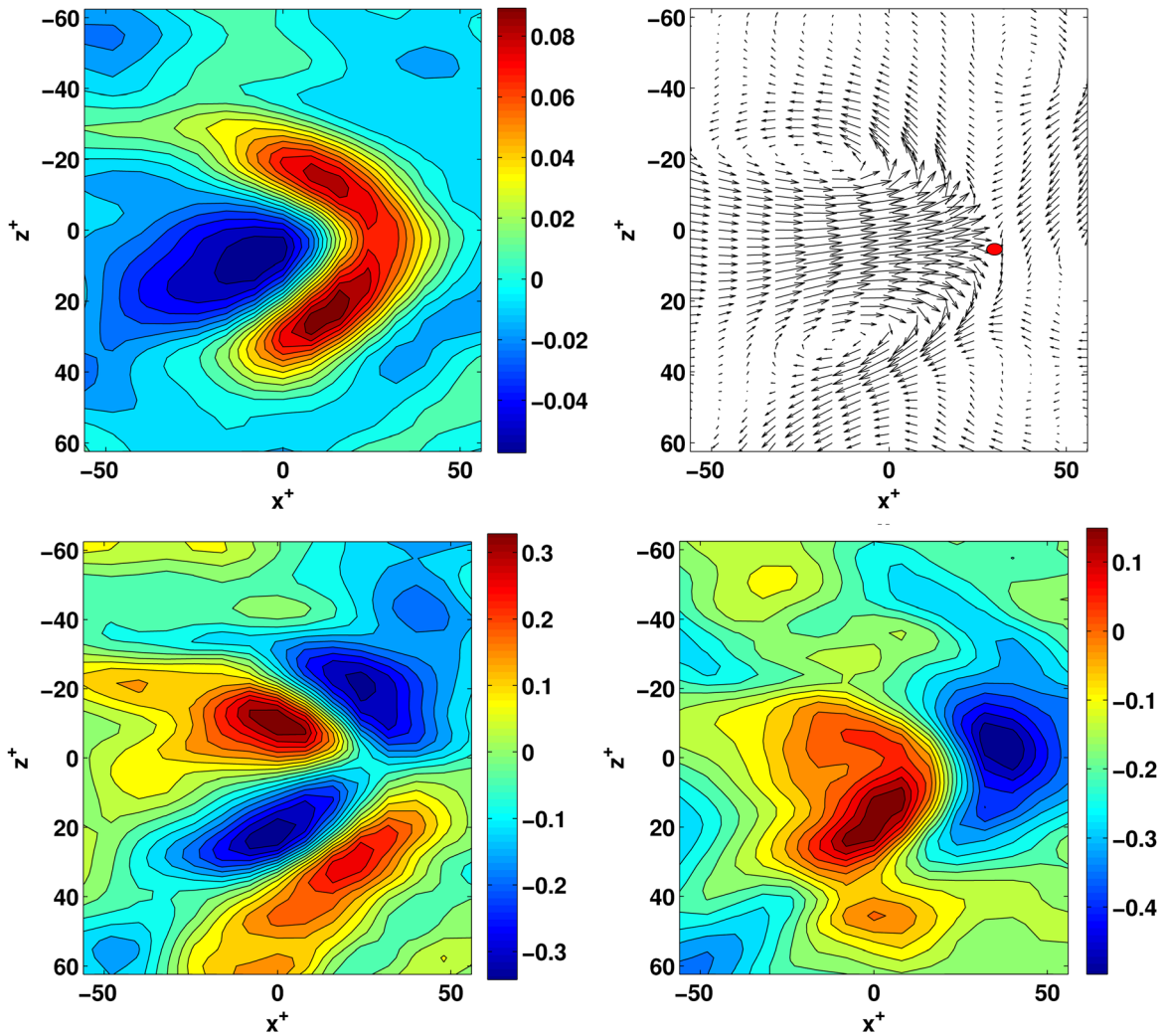

FIG. 14. (Color online) Statistics of the crescent vortices of first kind. Left to right and top to bottom: v', flow field (u', w') in (x^+, z^+)-plane, streamwise $\omega_x'\nu_\omega/u_\tau^2$ and spanwise $\omega_z'\nu_\omega/u_\tau^2$ vorticity components.

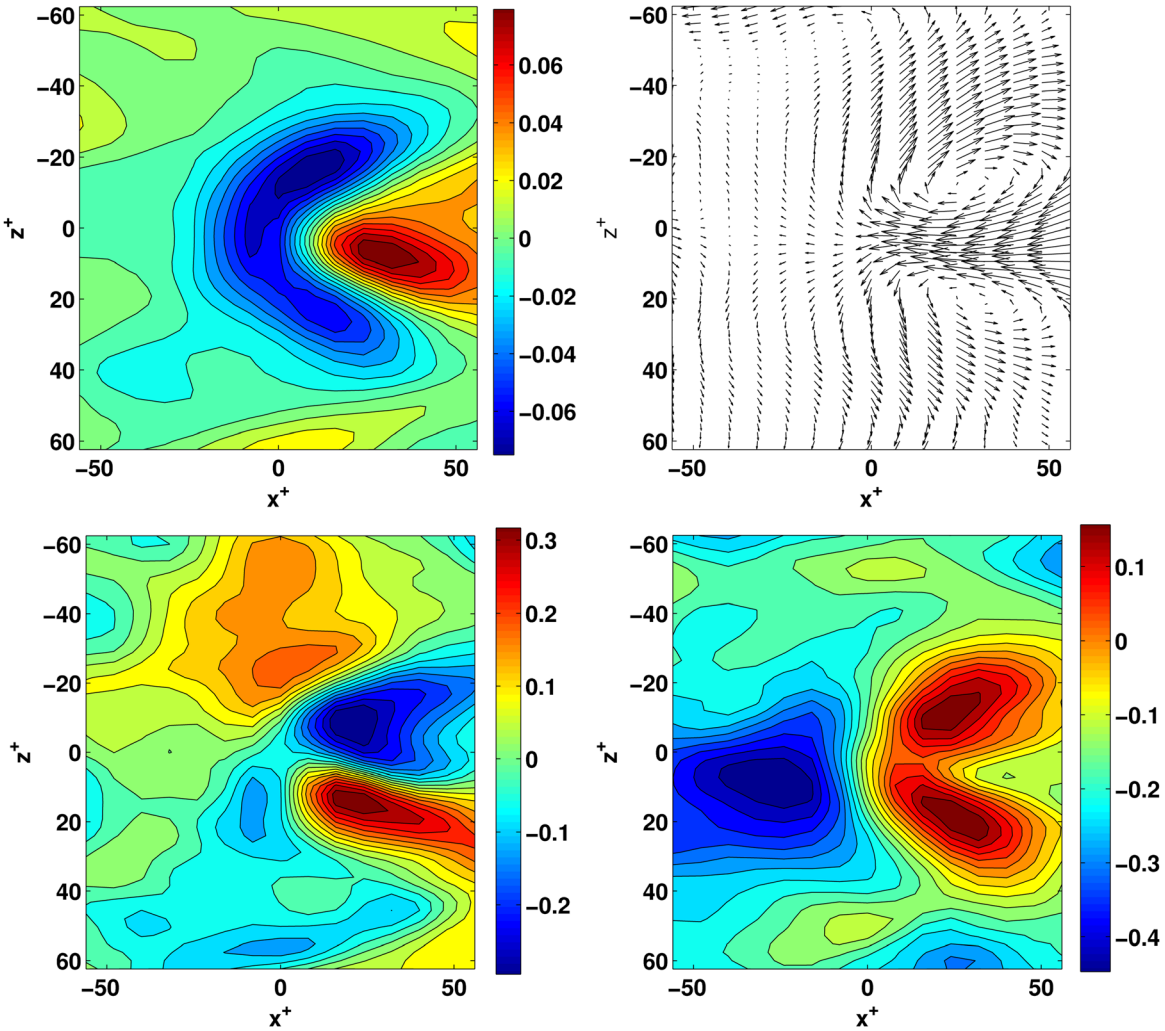

FIG. 15. (Color online) Statistics of the crescent vortices of second kind. Left to right and top to bottom: v', flow field (u', w') in (x^+, z^+)-plane, streamwise $\omega'_x\nu_\omega/u_\tau^2$ and spanwise $\omega'_z\nu_\omega/u_\tau^2$ vorticity components.

In Fig. 17, two patches of adjacent v', with alternating sign in the x-direction, were used to represent this spanwise vortex. Such a representation makes clear the generation process of streamwise vortices from the "deformation" of a spanwise vortex by the spanwise shear of the streaks.

The newly generated streamwise vortices enhance these streaks via the lift-up mechanism and produce three patches of positive Reynolds shear stress ($-u'v' \geq 0$), as shown in Fig. 17 and also in Figs. 9 and 12. It is worth noting that this is the only flow configuration in which the streamwise vortices, generated by the streaks, will in turn enhance the initial streaks via the lift-up mechanism and therefore enhance their generation process. If the initial spanwise vorticity was negative, these streamwise vortices will generate streaks having the opposite sign of the initial streaks. They will weaken these streaks and impede their generation process.

In this section we provide supporting evidence for this conceptual model. Namely, we will use the same method as above to decompose the streamwise velocity perturbation u' into a coherent part, representing the streaks, and an incoherent part and confirm the tilting and stretching role of the streaks. A simulation with $M_\infty = 20$ is also used to study the validity of these mechanisms for higher Mach numbers.

A. Tilting of spanwise vorticity by the streaks

First, the equation of the streamwise vorticity $\omega'_x = \frac{\partial w'}{\partial y} - \frac{\partial v'}{\partial z}$ reads

$$\frac{\partial \omega'_x}{\partial t} = \omega'_x\partial_x u' + \omega'_y\partial_y u' + \omega'_z\partial_z u' - \frac{\partial w'}{\partial x}\frac{d\bar{U}}{dy} - \omega'_x\left(\frac{\partial u'}{\partial x} + \frac{\partial v'}{\partial y} + \frac{\partial w'}{\partial z}\right) + \text{Baro.}\omega'_x + \text{Conv.}\omega'_x. + \frac{1}{R}\Delta\omega'_x.$$

The term Conv.ω'_x refers to the usual convection term. The term Baro.ω'_x refers to the barotropic torque due to the gradients of density and pressure. The first term on the rhs represents the stretching of the vorticity ω'_x while the second and third terms are the nonlinear tilting terms.

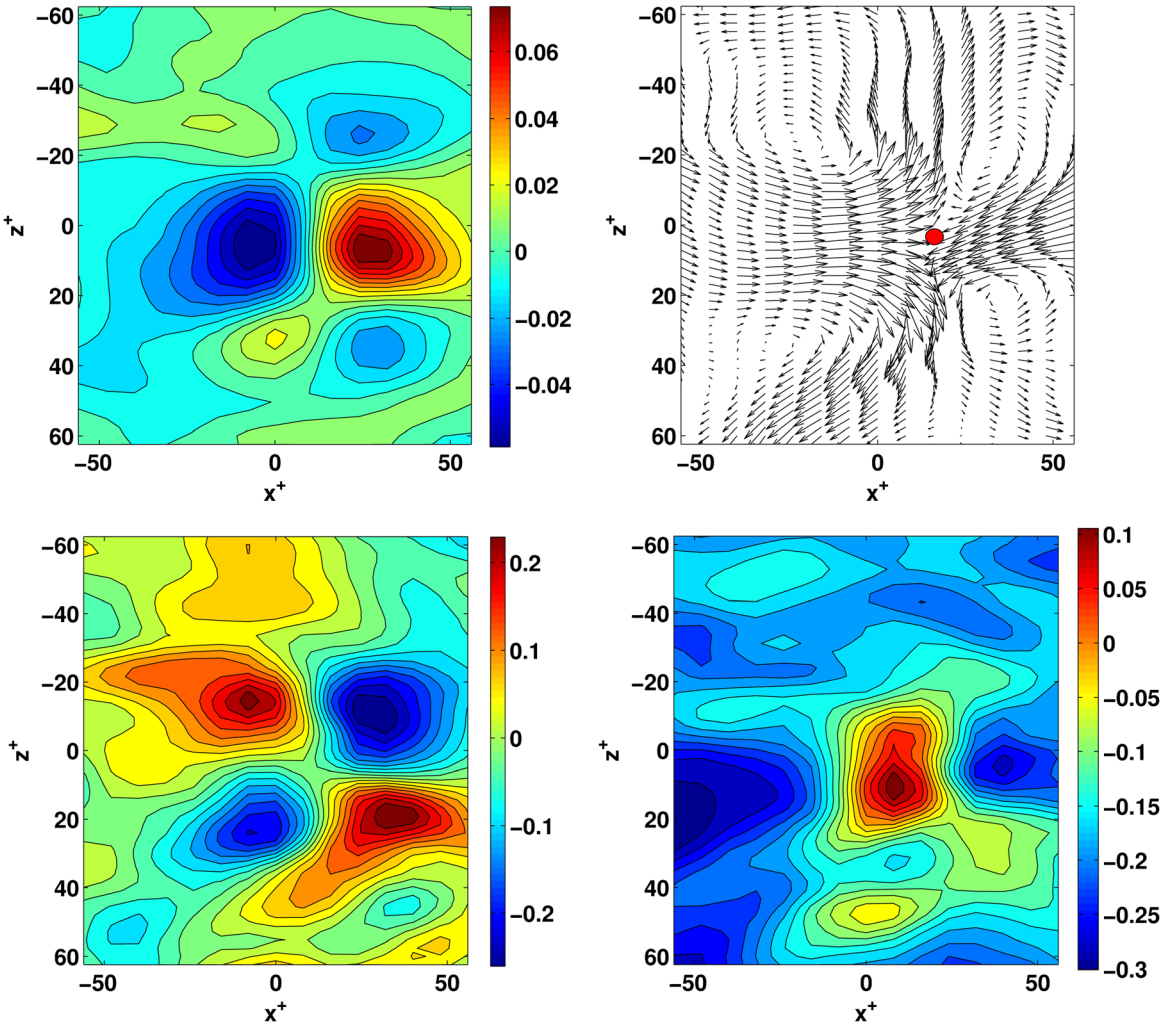

FIG. 16. (Color online) Statistics of the crescent vortices of both kinds. Left to right and top to bottom: v', flow field (u', w') in (x^+, z^+)-plane (the dot marks a stagnation point), streamwise $\omega'_x \nu_\omega / u_\tau^2$ and spanwise $\omega'_z \nu_\omega / u_\tau^2$ vorticity components.

The term $-\frac{\partial w'}{\partial x}\frac{d\bar{U}}{dy}$ contains the mean flow gradient effect $\frac{d\bar{U}}{dy}$. The last term accounts for the vorticity diffusion.

Since there is no mean streamwise vorticity in the boundary layer, its generation downstream of the inflow can only be explained by tilting of spanwise and/or wall-normal vorticity. Once generated, this vorticity will be stretched $(\omega'_x \partial_x u')$, advected, $(\text{Conv}.\omega'_x)$ interact with the mean profile $\left(\frac{\partial w'}{\partial x}\frac{d\bar{U}}{dy}\right)$ and dissipated $\left(\frac{1}{R}\Delta\omega'_x\right)$. In the next paragraph, we focus on the nonlinear generation mechanism of ω'_x.

The contribution of a term, say A, to the production of the vorticity is determined by computing the quantity

$$< A, \omega'_x > = \int_{x,z} A\omega'_x \, dx \, dz.$$

If this contribution is positive, the term is a source term, otherwise it is a sink term. The contribution of all these terms was computed by post-processing the instantaneous results from the current simulation data of the flow field at step 2. This evaluation revealed that the tilting $\omega'_z \partial_z u'$ and the stretching $\omega'_x \partial_x u'$ are source terms whereas $\omega'_y \partial_y u'$ is a sink term, as shown in Fig. 18. Note that the contribution of the compressibility terms is negligible and it is not shown here.

The vorticity equation can be further simplified by noting that $w'_y \partial_y u' + w'_z \partial_z u' = -\partial_x w' \partial_y u' + \partial_z u' \partial_x v'$. The contributions of the tilting terms $\partial_z u' \partial_x v'$ and $-\partial_x w' \partial_y u'$ are shown in Fig. 19. The positiveness of the contribution of $\partial_z u' \partial_x v'$ shows that this term is a source term, with a maximum located around $y^+ \approx 18$.

Hence, the streamwise vorticity is generated by the tilting of the spanwise vorticity $\partial_x v'$ by the spanwise shear of the streamwise velocity $\partial_z u'$. This tilting mechanism is due to the spanwise shear of the streak component of the streanwise velocity u', as shown below.

Following the remark made in Sec. II B, a streak spanning the near-wall region can be represented by the coherent part of the streamwise velocity perturbation u', decomposed as follow:

$$u' = u_{\text{streaks}}(x, z, t, y) + u_{\text{inc}}(x, z, t, y)$$

and where the streaks are defined as

$$u_{\text{streaks}} = P_0(y) u_0(x, z, t)$$

with

$$u_0 = \int_{y=0}^{y_{y^+=60}} P_0(y) u'(x, y, z, t) \, dy, \quad u_{\text{inc}} = u' - u_{\text{streaks}}.$$

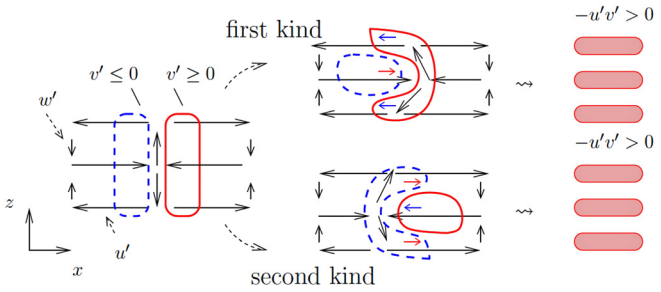

FIG. 17. (Color online) The conceptual model. A spanwise vortex, represented by two patches of $\pm v'$, is tilted by the spanwise shear of the streaks $\partial_z u'$. This deformation can yield one of the two kinds of crescent vortices. They both induce streaks u' (short arrows) through the lift-up mechanism and give positive Reynolds shear stress $-u'v'$. The quadrupolar flow (u', w'), around the initial spanwise vortex, is represented by the (black) arrows.

The polynomial P_0 keeps the same sign over the inner region and vanishes at the wall and at $y = y_{y^+=60}$. The simplest form satisfying these constraints is $P_0(y) \equiv y^2\left(y - y_{y^+=60}\right)^2$.

The tilting term $\partial_z u' \partial_x v'$ is decomposed as

$$\frac{\partial u'}{\partial z}\frac{\partial v'}{\partial x} = \left(\frac{\partial u_{\text{streaks}}}{\partial z} + \frac{\partial u_{\text{inc}}}{\partial z}\right)\frac{\partial v'}{\partial x} = \frac{\partial u_{\text{streaks}}}{\partial z}\frac{\partial v'}{\partial x} + \frac{\partial u_{\text{inc}}}{\partial z}\frac{\partial v'}{\partial x}.$$

As shown in Fig. 20, the contribution of the streaks to the tilting of the spanwise vorticity is not only positive (source term) but also dominates the contribution of the incoherent part and accounts for almost all the tilting mechanism for $y^+ \ge 10$.

B. Stretching of the spanwise vorticity

A second element of the conceptual model is the intensification of the spanwise vortex due to the spanwise stretching, driven by positive $\partial_z w'$. Using the same approach as before for the ω'_x-budget, we have found that the term $\omega'_z \partial_z w'$ in the ω'_z-equation

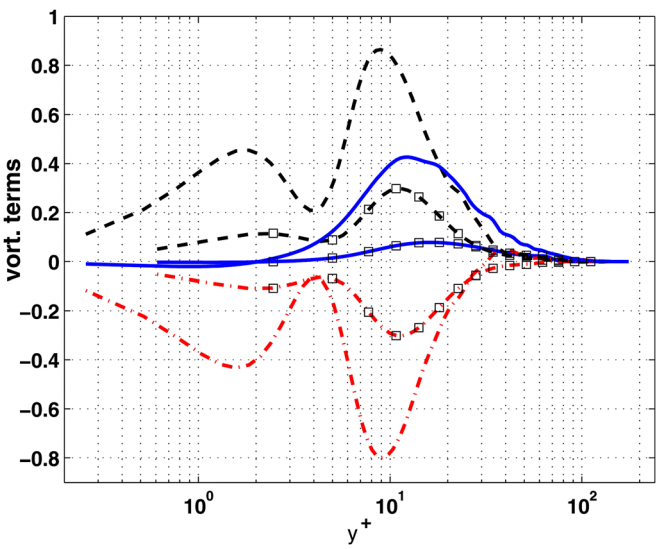

FIG. 18. (Color online) The stretching term $\omega'_x \partial_x u'$ is represented by a solid line (blue online), the tilting term $\omega'_z \partial_z u'$ is represented by a dashed line (black online), and the tilting term $\omega'_y \partial_y u'$ is represented by a dash-dotted line (red online). $M_\infty = 2.5$ (with squares) and $M_\infty = 20$.

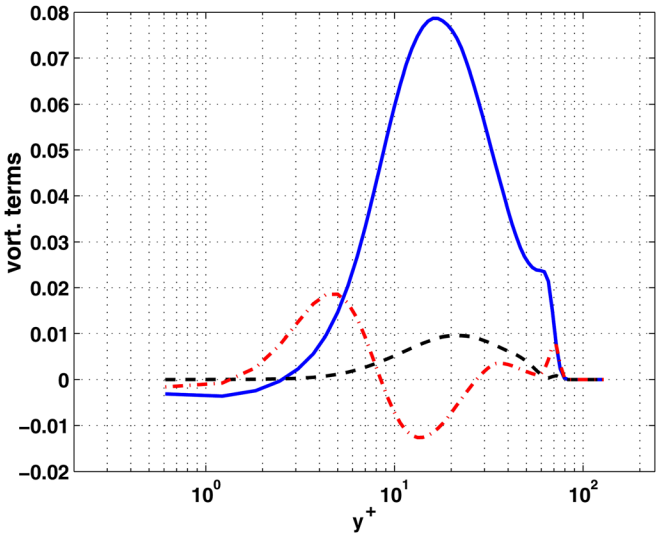

FIG. 19. (Color online) Stretching term $\omega'_x \partial_x u'$ represented by a solid line (blue online), the tilting term $\partial_z u' \partial_x v'$ is represented by a dashed line (black online), and the tilting term $-\partial_y u' \partial_x w'$ is represented by a dash-dotted line (red online).

$$\frac{\partial \omega'_z}{\partial t} = \omega'_z \partial_z w' + \omega'_y \partial_y w' + \omega'_x \partial_x w' - \frac{\partial w'}{\partial z}\frac{d\bar{U}}{dy} - \omega'_z\left(\frac{\partial u'}{\partial x} + \frac{\partial v'}{\partial y} + \frac{\partial w'}{\partial z}\right) + \text{Baro.}\omega'_z + \text{Conv.}\omega'_z + \frac{1}{R}\Delta\omega'_z,$$

is a source term, as shown in Fig. 21. The tilting terms have been written as $\omega'_y \partial_y w' + \omega'_x \partial_x w' = \partial_z u' \partial_y w' - \partial_z v' \partial_x w'$. This stretching in the spanwise direction of ω'_z is related to the compression, in the streamwise direction, of the spanwise vortex by the streaks, due to the negative $\partial_x u'$. In fact, when a high-speed streak impacts a low-speed streak, a stagnation point (in a frame of reference moving with the low-speed

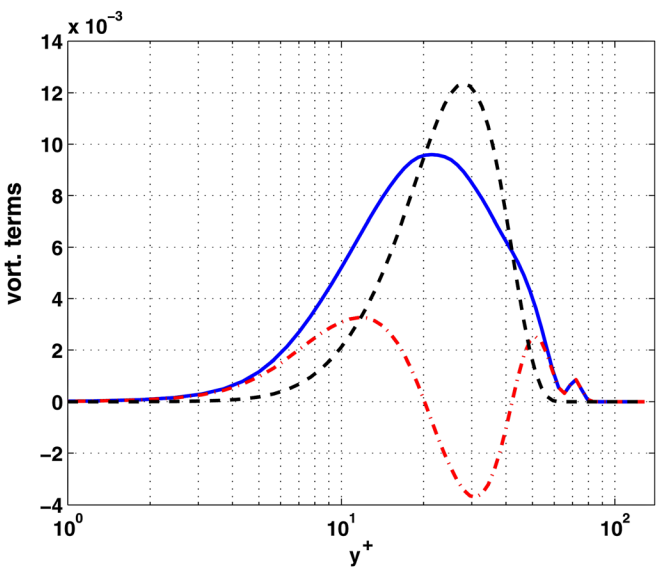

FIG. 20. (Color online) The role of the streaks in the tilting process. Solid line (blue online): $\frac{\partial u'}{\partial z}\frac{\partial v'}{\partial x}$, dashed line (black online): $\frac{\partial u_{\text{streaks}}}{\partial z}\frac{\partial v'}{\partial x}$, dash-dotted line (red online): $\frac{\partial u_{\text{inc}}}{\partial z}\frac{\partial v'}{\partial x}$.

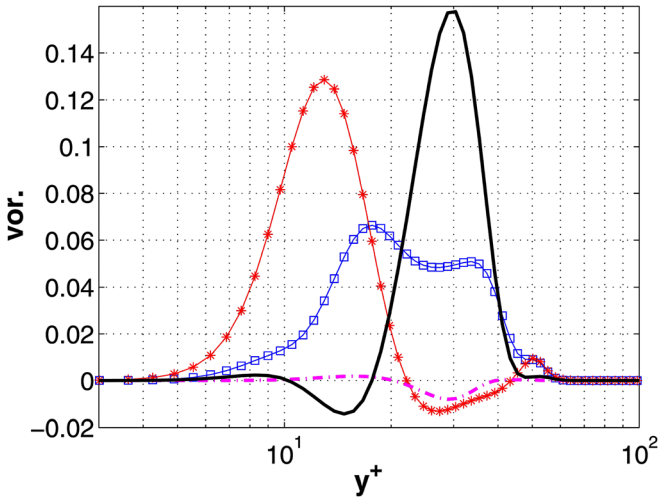

FIG. 21. (Color online) The ω_z' -equation. The stretching term $\omega_z'\partial_z w'$ is represented by squares (blue online), tilting term $\partial_z u'\partial_y w'$ is represented by a thick solid line (black online), and $-\partial_z v'\partial_x w'$ is represented by a dash-dotted line (magenta online). The linear term $-\partial_z w'\frac{d\bar{U}}{dy}$ is also shown with stars (red online).

streak) is formed and the flow is deviated in the spanwise direction. This (u', w') flow was shown in Fig. 16.

IV. DISCUSSION

In this section, we will present some points found through our work that reveal a close correspondence to well-known instantaneous experimental events obtained in the incompressible boundary layers.

Bogard and Tiederman[15] have shown that stagnation points are important because they are associated with regions containing high Reynolds shear stress production. These authors discussed the physical origin of these points, which, according to them, are a straightforward kinematic consequence of the impact of a high speed streak on the back of a low speed streak. Quoting these authors, "when a low speed fluid is lifted away from the wall by the streamwise vortices, it will present an obstacle onto which the high-speed fluid will impact and then flow around. This would cause the impingement point—termed in the present paper a stagnation point—and produce a shear layer with a strong negative velocity gradient in the streamwise direction." These shear layers are an important feature of the wall-bounded turbulence, and have been shown to be related to the turbulence production in fully turbulent flow at low Reynolds numbers (e.g., Ref. 12), as well as inside localized regions of turbulence. In addition to the negative streamwise gradient $\partial_x u'$, they are characterized by a positive $\partial_x v'$ (e.g., see Figs. 5 and 6 in Ref. 12), which is in agreement with the positive gradient $\partial_x v' \geq 0$, as shown in Fig. 16. Therefore, there is a similarity, both in topology and role, between these shear layer structures and the structure of the flow observed in this paper. Both represent localized regions where the turbulence is being produced.

Furthermore, by measuring the statistical properties of the vorticity field in a boundary layer flow, Balint *et al.*[16] found that the stretching of spanwise vorticity in the spanwise direction, due to a positive $\partial_z w'$, is more frequent than compression. According to Antonia and Kim,[17] it is plausible that this $\partial_z w'$ is the result of a wallward motion of fluid which, on encountering the wall, diverts in both the positive and negative z-directions. In the present study, the spanwise vorticity is also stretched in the z-direction (rather than compressed) due to the positiveness of $\partial_z w'$, which is related to the stagnation point events, shown in Fig. 16.

The existence of spanwise vortices with $\omega_z \geq 0$, being tilted by the streaks to generate streamwise vortices, shows that they are a building block of the self-sustained process of near-wall turbulence and suggests that manipulating the flow to create negative spanwise vorticity will reduce the turbulence activity. Several experiments (e.g., Ref. 18) have already been conducted in this field. A model has been proposed in Ref. 18 based on this result. It shows that the mean velocity gradient of the turbulent boundary layer close to the wall is reduced by the negative spanwise vorticity created in the near-wall region of the turbulent boundary layer over an oscillating wall.

Finally, it is worth mentioning that the local Mach number at $y^+ = 60$ is equal to 1.2 for the $M_\infty = 2.5$ case and increases up to 4.5 for the $M_\infty = 20$ case.[6] We have found that despite the difference in the free-stream Mach numbers and local Mach numbers, the coherent structures (crescent vortices) in the near-wall region for $y^+ \leq 60$ exhibit a strong similarity. This similarity is indeed expected since the statistics (rms values and energy budget) for compressible turbulent boundary layers with free stream Mach number ranging from 2.5 to 20 were shown to be similar.[6] Therefore, the coherent structures and the mechanisms at work are expected to be the same.

V. CONCLUSION

In this paper, we have shown that reducing the complexity of the full turbulent flow into a simplified flow consisting of only the coherent part of the near-wall turbulence brings out valuable insights into the coherent structures. This reduction is based on a few well connected steps. Step 3 serves as simplification of the full flow through restriction of the dimension of the system in the wall-normal direction. Step 2 is more faithful to the true dynamics of the wall region, yet both step 2 and step 3 are able to capture all the essential feature of the dynamics.

We have demonstrated that crescent-shaped vortical structures, which contain both signs of streamwise vorticity, populate the near-wall region. We have analyzed the flow around these vortical structures and shown that it is similar to the internal shear layer identified by other techniques in incompressible flows.[12] We have also provided a physical interpretation of the crescent-shaped vortical structure: a spanwise vortex with positive ω_z', surrounded by a quadrupolar flow having a stagnation point $u' \approx 0$, and stretched by positive $\partial_z w'$ in the z-direction and compressed by negative $\partial_x u'$ in the x-direction. This crescent vortical structure forms the basis of our proposed conceptual model, in which streamwise vortices are generated through tilting of positive ω_z' by the streaks $(\omega'_z\partial_z u')$ and then stretched in the x-direction $(\omega'_x\partial_x u')$. Through the lift-up mechanism, these streamwise vortices create streaks.

The role of these streaks in the generation of the spanwise vortices was not addressed in this paper. Therefore to present a complete self-sustained process for near-wall turbulence, the feedback of these streaks into the generation mechanism of spanwise vortices has to be investigated.

Although we have used a compressible boundary layer in this study, considering the results reported in Part I and some results presented here for different Mach numbers, the essential elements of the crescent-shaped vortical structures and their regeneration mechanisms discussed in the present paper apply to both compressible and incompressible boundary layers.

ACKNOWLEDGMENTS

We thank the referees for their invaluable insight and constructive commentary, which ultimately improved the quality of the manuscript. This work is supported by the NASA Grant/Cooperative Agreement NNX08AB39A. The computer time has been provided by NASA Ames Research Center and by NSF TRAC program.

[1]R. L. Panton, "Overview of the self-sustaining mechanisms of wall turbulence," Prog. Aerosp. Sci. **37**, 341 (2001).
[2]R. J. Adrian, "Hairpin vortex organization in wall turbulence," Phys. Fluids **19**, 041301 (2007).
[3]J. Jeong, F. Hussain,W. Schoppa, and J. Kim, "Coherent structures near the wall in a turbulent channel flow," J. Fluid Mech. **332**, 185 (1997).
[4]J. Jimenez and A. Pinelli, "The autonomous cycle of near-wall turbulence," J. Fluid Mech. **389**, 335 (1999).
[5]J. Jimenez and M. P. Simens, "Low-dimensional dynamics of a turbulent wall flow," J. Fluid Mech. **435**, 81 (2001).
[6]M. Lagha, J. Kim, J. D. Eldredge, and X. Zhong, "A numerical study of compressible turbulent boundary layers," Phys. Fluids **23**(1), 015106 (2011).
[7]M. J. Ringuette, M. Wu, and M. P. Martin, "Coherent structures in direct numerical simulation of turbulent boundary layers at Mach 3," J. Fluid Mech. **594**, 59 (2008).
[8]S. Pirozzoli, M. Bernardini, and F. Grasso, "Characterization of coherent vortical structures in a supersonic turbulent boundary layer," J. Fluid Mech. **613**, 205 (2008).
[9]M. Israeli and S. A. Orszag, "Approximation of radiation boundary conditions," J. Comput. Phys. **41**, 115 (1981).
[10]S. Xu and P. M. Martin, "Assessment of inflow boundary conditions for compressible turbulent boundary layers," Phys. Fluids **16**(7), 2623 (2004).
[11]P. J. Schmid and D.S. Henningson, "Stability and transition in shear flows," *Applied Mathematical Sciences* (Springer, New York, 2001).
[12]A. V. Johansson, P. H. Alfredsson, and J. Kim, "Evolution and dynamics of shear-layer structures in near-wall turbulence," J. Fluid Mech. **224**, 579 (1991).
[13]J. M. Hamilton, J. Kim, and F. Waleffe, "Regeneration mechanisms of near-wall turbulence structures," J. Fluid Mech. **287**, 317 (1995).
[14]W. Schoppa and F. Hussain, "Coherent structure generation in near-wall turbulence," J. Fluid Mech. **453**, 57 (2002).
[15]D. G. Bogard and W. G. Tiederman, "Characteristics of ejections in turbulent channel flow," J. Fluid Mech. **179**, 1 (1987).
[16]J. L. Balint, J. M. Wallace, and P. Vukoslavcevic, "The velocity and vorticity vector-fields of a turbulent boundary-layer. 2. Statistical properties," J. Fluid Mech. **228**, 53 (1991).
[17]R. A. Antonia and J. Kim, "Low-Reynolds-number effects on near-wall turbulence," J. Fluid Mech. **276**, 61 (1994).
[18]K. S. Choi, "Near-wall structure of turbulent boundary layer with spanwise-wall oscillation," Phys. Fluids **14**, 2530 (2002).